1

Introduction

1.1 An Overview of the ICT Process

Charge transfer is a fundamental step in many chemical and biological processes, including photosynthesis and metabolism [1–4]. The recent technological applications of charge-transfer–based materials include organic-light-emitting diodes (OLEDs), solar energy conversion, fluorescence sensing, nonlinear optical (NLO) materials, and so on [5–7]. The charge-transfer process may be divided into two broad categories. The transfer of charge from an electron-rich donor moiety to an electron-poor acceptor part located in different molecules is known as intermolecular charge-transfer process. However, if the donor and the acceptor belong to the same molecule, the phenomenon is called intramolecular charge-transfer (ICT) process. The ICT process generally occurs in the photoexcited state which a molecule reaches due to absorption of light of proper wavelength. The photoexcitation facilitates transfer of an electron from one part of a molecule/ion to its other part in the excited state, which makes the charge distribution in the excited state markedly different from that in the ground state. The through-bond ICT occurs in molecules in which the donor and the acceptor groups are connected through a π-electron bridge (Figure 1.1). In some rare cases, an intramolecular through-space charge transfer is observed, where the transfer of charge through the conjugative path is denied but donor and acceptor groups are in a favorable position for charge transfer. Although the intermolecular interaction mediated by through-space charge transfer dictates the properties of many π-stacked molecular systems, studies of intramolecular through-space charge transfer is scarce. In π-conjugated organic molecules comprising electron donor (D) and acceptor (A) subunits, the process has attracted a lot of attention due to their immense technological implications in organic electronics and photovoltaics [5–14]. Materials based on such organic molecules are potential candidates for use in OLEDs, field-effect transistors, dye-sensitized solar cells, to name a few. In this book, our focus is mainly on the excited-state ICT in stable organic molecules as well as in inorganic complexes. A few examples of the electron-transfer process in biomolecules have also been discussed. The signatures of ICT, spectroscopic techniques, and theoretical tools employed to study this process are also mentioned. It is now known that

Intramolecular Charge Transfer: Theory and Applications,
First Edition. Ramprasad Misra and S. P. Bhattacharyya.

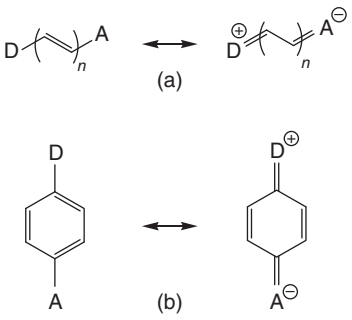

Figure 1.1 The intramolecular charge-transfer processes (a) in a (poly)ene system and (b) in an aromatic donor–acceptor molecule. Donor (D) to acceptor (A) charge transfer occurs in the excited state through the π-electron bridge to form an ICT state of higher dipole moment.

excited-state ICT in organic molecules may give rise to dual emission in its electronic spectrum. The peak seen at the blue end of the emission spectrum is generally believed to be arising from a locally excited (LE) state of the molecule, while the peak at the red end is generally assumed to bear the signature of an ICT species formed in the excited state. The ICT process generally occurs in polar solvents and the Stokes-shifted ICT fluorescence is observed due to solvent stabilization in the excited state [15]. In Figure 1.2, the potential energy surfaces (PES) for the ground state S_0 and the first two excited states (S_1, S_2) have been depicted along with the LE and ICT states. The vertical coordinate represents energy, while the horizontal coordinate (ξ) comprises all molecular changes accompanying the LE → ICT reaction, such as changes in bond lengths and bond angles. In the given example, excitation of the molecule leads it to the S_2 state, which relaxes through internal conversion to the equilibrated LE state. The ICT reaction proceeds from the LE to the ICT state that has a

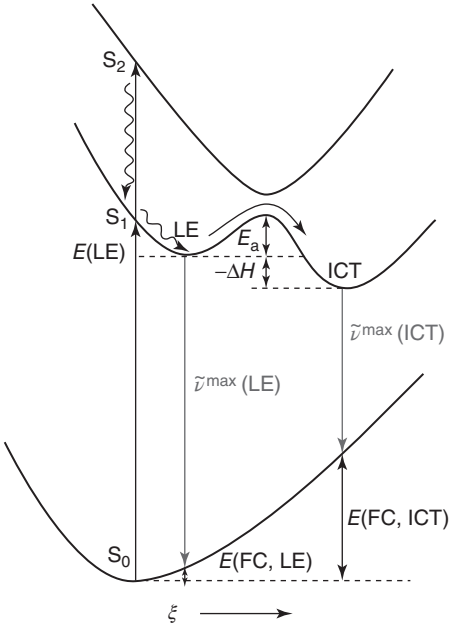

Figure 1.2 Schematic representation of intramolecular charge transfer (ICT) process in a model system. In the given scheme, excitation leads the molecule to the S_2 state from which it reaches the S_1-LE state through internal conversion. The ICT state is accessible through the S_1-LE state. Emission form both the LE and ICT states leads to dual emission from the molecule. (Druzhinin *et al*. 2010 [15]. Reproduced with permission of American Chemical Society.)

reaction barrier E_a and an enthalpy difference of ΔH. Fluorescence from the LE and ICT states reaches the corresponding Franck–Condon states E(FC, LE) and E(FC, ICT). This gives rise to dual fluorescence with emission maxima of $\tilde{\nu}_{max}$(LE) and $\tilde{\nu}_{max}$(ICT), respectively. Lippert and coworkers reported the dual fluorescence in 4-*N*,*N*-dimethylaminobenzonitrile (DMABN) for the first time in 1962 [16]. The debate continued regarding the origin of the dual emission of DMABN for some years. Most of the studies accepted that the observed dual emission from DMABN is due to excited-state ICT from the dimethylamine to the cyano group through the π-electron bridge. Later on, many congeners of DMABN were put under the scanner for deciphering or decoding the nature of the ICT process and its dynamics. Many experimental or theoretical studies or both have been devoted to investigate the charge-transfer mechanism in different organic molecules. The early experimental and theoretical results on the ICT process support a twisted intramolecular charge-transfer state (called TICT state) [16]. In the framework of the TICT model, the dual emission of an ICT probe originates from the primary excited, called LE, state as well as from the ICT state. The ICT state is accessible only by an adiabatic photoreaction from the LE state that includes rotational motion around the bond connecting the donor and acceptor moieties. If there is no energy barrier between the LE and ICT states, the excited-state relaxation can occur extremely rapidly, resulting in emission from the ICT species only. Although the TICT mechanism is till date the most popular concept in describing the structure of the excited state, this model was challenged by several groups. Later on, several other models, like planar intramolecular charge transfer (PICT), rehybridized intramolecular charge transfer (RICT), and wagging intramolecular charge transfer (WICT), were proposed by several groups to explain their experimental results. For example, Domcke and coworkers put forward a RICT model to account for the formation of the ICT state of DMABN and its analogs. Later on, the formation of a charge-transfer state from a rigid molecule, *N*-phenylpyrrole (PP) and its free analog, fluorazene phenylpyrrole (FPP) put a question mark on the validity of the TICT model. The similarity in spectral signatures of these molecules could not be explained using the TICT model. This led to the proposal of a PICT mechanism to explain the spectroscopic response of the aforesaid molecules. There are several other examples that support the fact that the ICT state of the molecule does not need to be twisted. The origin and drawbacks of some of these models have been described in Chapter 2.

Another point regarding the formation of the ICT state that is still under intense debate is the pathways of the charge-transfer process, that is, the mechanism through which the ICT process in a molecule occurs. Several high-level calculations and state-of-the-art experimental techniques have been used to settle this issue. In spite of several studies that describe the PES of the ICT process, this issue is yet to be settled amicably. A current account of this topic has been described briefly in Chapter 2. The charge-transfer studies in some other molecules, including rhodamine derivatives, coumarin, oxazine, flavin, Nile red, and so on, are discussed in Chapter 2.

1.2 Experimental and Theoretical Studies of the ICT Process

As we mentioned earlier, several studies have been devoted to explore the structure and mechanism of formation of the ICT state. Initially, steady-state UV–visible absorption and emission spectroscopy have been widely used for studying the ICT phenomenon in several organic molecules as dual fluorescence is a major observation of the ICT process. Later on, time-resolved spectral techniques, including, picosecond (ps) time-resolved fluorescence, femtosecond transient absorption (TA) and fluorescence upconversion spectroscopies are used by the scientific community to study the ICT process. Recently, Fleming and coworkers [17] have used a combined ultrafast electronic pump and infrared (IR) probe spectroscopy to study the excited-state CT. Gaffney and coworkers [18] have used polarization-resolved UV pump–mid-IR probe spectroscopy, in conjunction with time-dependent density functional theory (TDDFT) calculations to investigate the dynamics of charge-transfer–induced intramolecular rotation in julolidine malononitrile (JDMN), an ICT probe. Of late, Terahertz (THz) spectroscopy [19] is being used to measure the ICT in a molecule directly. When the ICT process occurs in a molecule, electronic charge moves from one end to another, which will undergo acceleration, resulting in radiation of electromagnetic (EM) pulses. If the charge-transfer process occurs on ps timescale, the radiated EM pulse will fall in the THz region of the spectrum. There are some phenomena similar to ICT, like energy transfer, intramolecular proton transfer (IPT), and so on that has similarity to this process but are different in nature. Dual fluorescence has also been observed in molecules undergoing excited-state intramolecular proton transfer (ESIPT). Although ESIPT is also a charge-transfer process, it is sometimes necessary to distinguish between the ICT and IPT processes occurring in a molecule. It has been seen that the IPT process occurs on a much faster timescale compared to the ICT process. On the other hand, in an ESIPT process, the hydrogen donor and acceptor groups must be present within a certain distance of each other, while ICT can occur even if the donor and the acceptor groups in a molecule are placed quite a distance apart either by a "through-bond" process mediated by a π-electron bridge or by a "through-space" interaction. It is now known that both the ICT and ESIPT processes are dependent on the solvents. One can therefore distinguish these two processes by changing the medium, which in turn will affect their spectroscopic properties.

During the ICT process, the electronic charge distribution of a molecule changes, generally resulting in an ICT species with higher dipole moment compared to its ground-state counterpart. The idea of the formation of a higher dipole moment species has also been supported by the fact that in polar solvent the ICT reaction becomes faster due to better stabilization of the polar ICT species in polar medium. The formation of the ICT process in a molecule is also indicated through the redshifted emission as one goes from a nonpolar to a polar solvent. Although many of the ICT molecules show dual emission in polar solvents, not all of them show dual emission. It is believed that due to ICT the non-radiative

deactivation channels (like solvent relaxation) become active, finally decreasing the emission quantum yield. The properties of the medium play a crucial role in determining the rate of formation of the ICT state as well as its structure.

It is worth mentioning here that not all ICT molecules show redshifted emission maxima upon photoexcitation. Molecules with zwitterionic ground state gets charge transfer in the excited state, generally resulting in a species with lower dipole moment than that in the ground state. This may result in a blueshift in their emission maxima. For example, betaine-30, also known as Reichardt's dye (Figure 1.3) shows negative solvatochromism [20]. This was explained by the change in its dipole moment in the ground state to that in the excited state. The molecule remains in a charge-transferred zwitterionic (D^+-A^-) state in the ground state that turns into a D-A state upon photoexcitation. The dipole moment of the betaine-30 is reported to be about 15 D and 6.2 D in the ground and excited states, respectively.

Several theoretical calculations have been employed to study the ICT process. Initially, semiempirical methods were used by several groups to explore the structure of the ICT state. Later, Hartree–Fock (HF), density functional theory (DFT), complete active space self-consistent field method (CASSCF) and second-order correction to CASSCF (CASPT2) level of theories were employed either alone or in conjunction with experimental studies to explore the ICT process in the excited state. Many of these theories now can reproduce the experimental results on the ICT process accurately. It is now known that standard DFT functional like B3LYP in many cases failed to reproduce the spectral properties of charge-transfer–based molecules. Therefore, several studies have devoted to propose new DFT functional and basis set combinations to study the ICT process. Some of these studies are discussed in the following

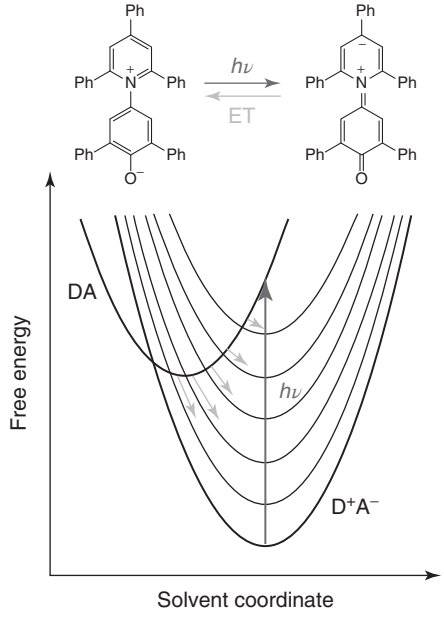

Figure 1.3 The free energy curves of the ground (S_0) and first excited (S_1) states of betaine-30. The vibrational levels and possible ET mechanism are also shown. (Kumpulainen *et al*. 2017 [20]. Reproduced with permission of American Chemical Society.)

chapters of this book. Initial theoretical studies involved optimization of the ground state, followed by calculation of spectroscopic properties using the ground-state geometry with certain approximation. Of late, optimization of the excited-state geometry using configuration interaction singles (CIS), TDDFT, and CASSCF level of theories has been undertaken to understand the physical nature of the charge transfer in specific organic molecules. It is apparent that in a molecule the formation of the ICT state from the LE state competes with the radiative deactivation process. These states occupy different regions of the PES of the relevant molecule. To understand and interpret the phenomenon unambiguously, the details of the PES of these molecules in the ground and excited states are therefore necessary. Of late, theoretical calculations at the CIS, TDDFT, CASSCF, and CASPT2 level of theories and femtosecond pump-probe spectroscopy have been essential tools in such endeavors. A detailed description on theoretical studies on ICT can be found in Chapter 3.

Electron transfer (ET) reaction can be considered as one of the simplest chemical reactions occurring in nature. Initially, the classical Marcus theory, proposed during the mid-fifties of the previous century became very popular. In the model described by Marcus theory, the free energy of the reactant (R) and product (P) goes along the reaction coordinate, comprising both solvent and intramolecular modes [21]. The horizontal displacement, as shown in Figure 1.4, accounts for the difference in equilibrium geometries of the reactant and product states and is quantized by the reorganization energy (λ). On the other hand, the vertical displacement represents the driving force of the reaction and is denoted as $-\Delta G_{ET}$. The reorganization energy can be further divided into contribution from the solvent and intramolecular modes. In classical Marcus theory, the ET reaction is considered as a thermally activated process and the rate of this reaction (k_{ET}) can be expressed in an Arrhenius-type equation, as shown in Equation 1.1.

$$k_{ET} = A \exp\left[-\frac{(\Delta G_{ET} + \lambda)^2}{4\lambda k_B T}\right] \tag{1.1}$$

where k_B is the Boltzmann constant and T is the absolute temperature.

From Equation 1.1, three conditions can arise: (i) In the normal region, $-\Delta G_{ET} < \lambda$, the values of k_{ET} increases with the driving force. (ii) In the

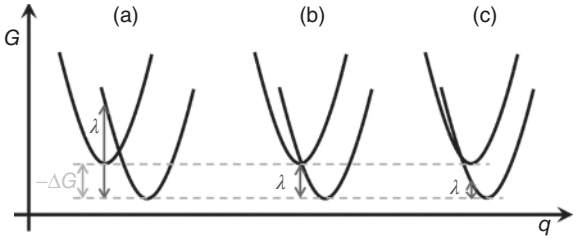

Figure 1.4 Potential energy curves along the reaction coordinate, *q*, for the reactant and product states. The curves a, b, and c represent the normal, barrier-less and inverted Marcus regions, respectively (see text for details). (Pelzer and Darling 2016 [22]. Reproduced with permission of Royal Society of Chemistry.)

barrier-less region $-\Delta G_{ET}$ is almost equal to λ, the k_{ET} value reaches the maxima. (iii) In the inverted region, $-\Delta G_{ET} > \lambda$, the values of k_{ET} decreases with increasing driving force.

Later, several semiclassical and quantum mechanical descriptions of the ET process were considered [20, 22]. Fermi Golden rule [23] is one of the popular models to study the ET process. Sumi–Marcus theory [24] of ET considers the possibility of the ET process taking place faster than the solvent relaxation by splitting the reaction coordinate into fast and a slow coordinates, where they are associated with the relaxing intramolecular modes and with the solvents, respectively. Some of the methods to find the rate of electron-transfer process are discussed in Chapter 3. Recently, Manna and Dunietz [25] studied the rate of photoinduced charge-transfer processes within dyads consisting of porphyrin derivatives in which one ring ligates a zinc (Zn) metal center and where the rings vary by their degree of conjugation.

The separation of charge that follows the ICT process generally enhances the dipole moment of the system in the excited state with some exceptions, like betaine-30 (discussed in this chapter). So, it is quite likely that the ICT species will be stabilized progressively with increase in the polarity of the medium as polar solvents surround the polar probe to exert stability to the probe molecule. The signatures of the ICT process are therefore expected to be more recognizable in strongly polar solvents. A solute (probe) interacts with the solvent in different ways. In suitable cases, it can form molecular clusters of specific sizes and stoichiometries through specific interaction (mostly through hydrogen bonding) with the solvent molecules. On the other hand, the solute molecules may be solvated through the dielectric property of the solvent. This process is called macroscopic or bulk solvation. Both specific or microscopic solvation and macroscopic solvation in dielectric continuum could shape the photophysics of the solute. Many experimental, quantum chemical studies and simulations have been therefore undertaken by the scientific community to unravel the microscopic details the solvent effects on the ICT process [26–38]. It is now known that investigations of structure and dynamics of hydrogen-bonded molecular clusters provide us with the opportunity to understand the effect of the bulk solvation systematically. The studies of cluster formation between solvent and solute molecules also enable one to understand many complex physical and chemical processes from a molecular point of view, which is not possible in the study of bulk solvents. The investigations on the formation of molecular clusters have been fueled due to advent of experimental methods like the mass-selective resonance two-photon ionization (R2PI), rotational coherence spectroscopy (RCS), two-photon ionization and IR ion depletion (IR/R2PI) spectroscopy, among others [39]. A large volume of research has been devoted to explore the molecular clusters in the ground state. Of late, invention of many state-of-the-art time-resolved spectroscopic techniques, like femtosecond TA spectroscopy, femtosecond time-resolved fluorescence spectroscopy, time-resolved vibrational spectroscopy, and so on, have enabled the scientific community to study hydrogen bonding in the excited states. The effect of the medium polarity and hydrogen bonding ability on the ICT process on some molecules is discussed in Chapter 4. Studies of the ICT process is

generally done in solution. However, a few studies of ICT have been reported in literature either in the gas phase or in solid state. A few representative examples of ICT studies in the gaseous and solid states can be found in Chapters 2 and 4.

As mentioned earlier, several new ICT molecules are being reported in literature to understand the ICT process in detail that could be useful in using them for technological applications. Zhao *et al*. [40] have reported the photoinduced ICT process in thiophene-π–conjugated donor–acceptor compounds. As thiophene has lower delocalization energy than benzene, the authors hoped that the former could be a better spacer for π-conjugation in ICT molecules. In fact, several compounds containing thiophene ring have been investigated for possible use in optoelectronic devices, such as NLO, OLEDs, and dye-sensitized solar cells [41–43]. To test their hypothesis, the authors compared the spectral properties of QTCP with its benzene-bridged analog QBTP (Figure 1.5). They assigned the large Stokes shift and strong solvatochromism of these molecules to the formation of the ICT state. They also found that the electron-withdrawing ability of the substituents at the thienyl 2-position affected the ICT process of the molecules studied. In addition to this, they also observed emission from the S_2 state of these molecules, which they confirmed through their fluorescence excitation spectra.

Studies of the ICT process led to the proposal of several theoretical models to mostly predict the rate of the ICT process. Some of these models have been discussed in Chapter 3. Recently, Ivanov and coworkers [44] have reported their simulation studies of ultrafast charge recombination in ion pairs formed through intramolecular electron-transfer process in the light of free-energy-gap law. They simulated the kinetics of charge transfer and ensuing ultrafast charge recombination within the framework of multichannel stochastic model that considers reorganization of both the solvents and a number of intramolecular high-frequency vibrational modes. They described the solvent relaxation in terms of two relaxation modes. The authors found that for ultrafast charge recombination the free-energy-gap law strongly depended on parameters like electronic coupling, reorganization energy of the intramolecular high frequency vibrational modes, as well as the vibrational and solvent relaxation times.

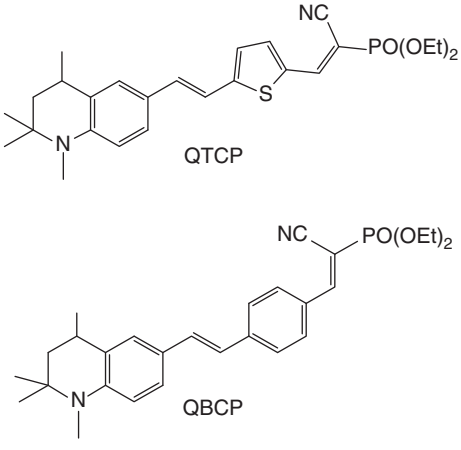

Figure 1.5 The chemical structure of QTCP and QBTP.

They also found that the semilog dependence of the charge recombination rate constant on the free-energy gap varied from a parabolic shape to an almost linear one, while the electronic coupling was increased and the vibrational relaxation time was decreased. The authors predicted that the dynamical solvent effect in charge recombination was large in the area of strong exergonicity, while the effect was small in the area of weak exergonicity.

As mentioned earlier, the properties of the medium play a crucial role in determining the properties of an ICT molecule. Dube and coworkers [45] have reported that the internal motions of hemithioindigo (HTI) photoswitches could be controlled through a change of solvent. The control of the internal motions of molecules using stimuli from outside is important for generation of responsive as well as complex molecular behavior and functionality. Photoswitches that react to light reversibly in a specific way are used as "engine" unit to trigger specific motion as well as events in functional molecular and biological systems [46–48]. HTI derivatives typically consist of a central double bond that functions as a bridge between the thioindigo fragment and a stilbene fragment via one additional single bond. After photoexcitation, unsubstituted HTI derivatives undergo de-excitation in which rotation of the double bond occurs, with additional pyramidalization of the corresponding carbon atoms. The presence of a single C—C bond in these molecules raises the possibility of rotation of this bond during the de-excitation process. Simultaneous rotation of the single and double bonds, called hula-twisting, is generally not considered to take place during de-excitation of unsubstituted HTI derivatives. To test the possible formation of TICT states, the authors considered four HTI derivatives acronymed *Z*-1 to *Z*-4 (Figure 1.6). HTI derivatives *Z*-1 to *Z*-3 possess substituents in both *ortho*-positions of the stilbene fragment. They used the planar derivative HTI

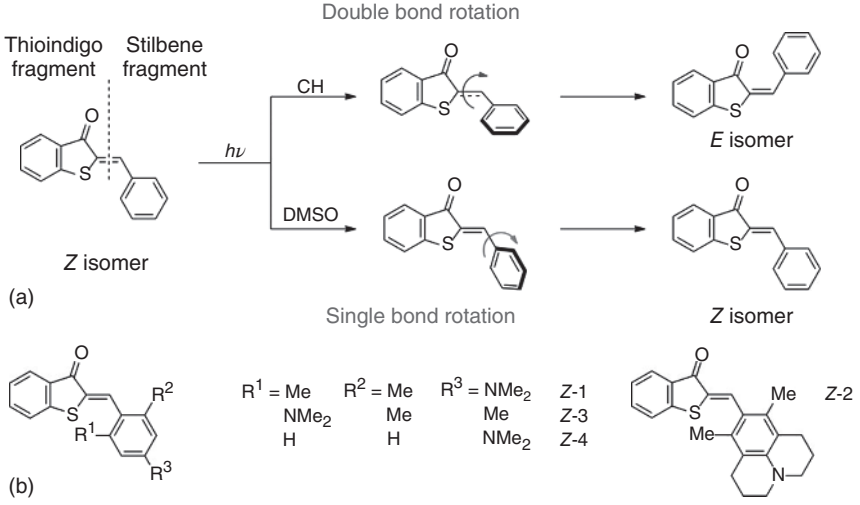

Figure 1.6 (a) Possible light-induced motions of the HTI derivatives, as proposed by Dube *et al*. (b) The chemical structures of the HTI photoswitches *Z*-1 to *Z*-4. (Wiedbrauk *et al*. 2016 [45]. Reproduced with permission of American Chemical Society.)

Z-4 as control, which does not undergo the TICT process in the excited state. All the four derivatives have strong electron-donor dialkylamino substituent (the electronic effect of additional alkyl substituents in *Z*-1 to *Z*-3 was considered to be not much). The twofold *ortho*-substitution in *Z*-1 to *Z*-3 resulted in a significant twist along the single-bond axis that could be measured using crystal structure analysis. The authors found that the dihedral angle around the rotatable single bond was highest for *Z*-1, with a value of 75°. The aforesaid dihedral angles for *Z*-2 and *Z*-3 were found to be 60° and 32°, respectively. Their planar analog *Z*-4 showed the dihedral angle to be 7° in its crystal structure analysis. The authors studied the chemical shift of indicative proton signals in ^{1}H NMR spectra of *Z*-1 to *Z*-3 that showed a similar twist of these molecules even in solution phase. As expected, the planar molecule HTI *Z*-4 showed moderate solvatochromism in both absorption and fluorescence. The absorption spectra of HTIs *Z*-1 to *Z*-3 also showed moderate solvatochromism, although somewhat broader than their planar analog *Z*-4. The fluorescence spectra of HTIs *Z*-1 and *Z*-2 were affected significantly due to the change in the polarity of the medium. In polar solvents, those molecules showed Stokes shift of more than 200 nm. Dual emission of *Z*-1 and *Z*-2 were observed in polar solvents like dimethyl formamide (DMF), dimethyl sulfoxide (DMSO) and acetonitrile. The steady-state absorption and emission behavior of HTI *Z*-3 was quite similar to HTIs *Z*-1 and *Z*-2, although the authors did not find any clear indication of dual emission of this probe. The authors undertook time-resolved absorption, time-resolved emission, and quantum yield measurements to understand the photophysics of the aforesaid molecules in detail. They followed the ultrafast kinetics taking place after photoexcitation of HTIs *Z*-1 to *Z*-4 in different media at 22 °C by TA spectroscopy with 150 fs resolution. Although the fitting of the time-resolved absorption curve of HTI *Z*-4 resulted in several timescales, the authors identified the important processes to describe the excited-state dynamics of these molecules. For this molecule, very fast nuclear motions and solvent reorganization were observed due to photoexcitation to the Franck–Condon (FC) region before reaching the relaxed first excited state (S_{1Min}). The S_{1Min} was identified in all the solvents studied through small redshifted ground-state bleaches and simulated emissions. The redshift increases with increasing solvent polarity. The authors argued that the decay of this electronic excited state to be related to the *Z*/*E* photoisomerization of this molecule (HTI *Z*-4). The rate of photoisomerization of HTI *Z*-4 was found to be solvent dependent, which decreased with increasing solvent polarity. The slowing down of photoisomerization with increase in the polarity of the solvents was attributed to the significantly polar nature of the S_{1Min}. However, no indication of formation of the TICT state was observed in HTI *Z*-4. For twisted HTI derivative *Z*-1, the initial absorption behavior in nonpolar solvents like cyclohexane was found to be quite similar to its planar counterpart HTI *Z*-4, although the decay of the excited-state features and appearance of *E* isomer absorption in this molecule was found to be faster than that in HTI-*Z*-4. The authors argued that the steric interactions imposed by the *ortho*-substituents in HTI *Z*-1 could be the reason for fast isomerization of this molecule in nonpolar solvents. In moderately polar solvents like dichloromethane (CH_2Cl_2), the time-resolved absorption profile of

HTI *Z*-1 varied significantly that of its planar counterpart. Dual emission of *Z*-1 and *Z*-2 were observed in polar solvents like DMF, DMSO, and acetonitrile. They also found that the excited electronic state had redshifted simulated emission and new excited-state absorption (ESA) features. This new excited state was found in HTI *Z*-1 in every polar solvent used for the study and the time constant of the relatively longer lived state was connected to the decay of S_{1Min}, while the amplitude is determined by the properties of the solvent as well as the specific decay time. The authors found that the new excited state (they call it T as it was only observed in the twisted HTI derivatives) got stabilized significantly with increase in solvent polarity. This indicated that the new excited state was highly polar and could possess significant charge-transfer character, a characteristic of the TICT state. Similar studies were carried out for HTIs *Z*-2 and *Z*-3, which also indicated the formation of TICT states in these molecules. The steady-state absorption and emission, time-resolved absorption and emission spectral studies, and quantum yield measurements of the probe led the authors to conclude the following. For planar HTI derivative *Z*-4, the de-excitation occurs through the photoisomerization of the double bond using the conical intersection ($CoIn_{S2}$) between the second excited state (S_2) and the ground state (S_0). The excited population leaves the initially reached S_{1Min} state and crosses a barrier to reach the S_2 hyperpotential surface. Finally, it reached the $CoIn_{S2}$ from which the transition to the S_0 state occurs. The behavior of HTI *Z*-4 is solvent independent. In twisted HTI derivative *Z*-1, the excited-state behavior is solvent dependent. In nonpolar solvent cyclohexane, the excited TICT state is not accessible and the de-excitation proceeds through the double-bond photoisomerization pathway. This led to fluorescence of HTI *Z*-1 from the S_{1Min} of this molecule in cyclohexane. In solvents with medium polarity (CH_2Cl_2), the TICT state of HTI *Z*-1 is stabilized significantly and gets populated upon photoexcitation. A strong fluorescence of this molecule from the TICT state occurs in CH_2Cl_2. Increasing solvent polarity further (e.g., DMSO) stabilizes the TICT more which leads to opening of another radiation-less de-excitation pathway through rotation around the single bond. The depopulation of the TICT state in DMSO becomes rapid and another blueshifted emission from S_{1Min} is observed in this solvent. All these results are schematically shown in Figure 1.7. The results presented by the authors showed that an unprecedented control over the photoinduced intramolecular rotations could be achieved for the HTI photoswitches through change in solvent polarity.

It is worthwhile to note here that just connecting the donor and acceptor moieties through the π-electron bridge in a molecule is not enough for ICT to occur in the exited state. Dube and coworkers [49] have studied the structural and electronic factors required for formation of excited ICT state in a series of HTI dyes (Figure 1.8). These dyes have been studied extensively for possible use as photoswitches that have advantages like high thermal bistability, fatigue-resistant switching, and visible light responsiveness. The TICT process is reported to be a second de-excitation pathway that is complementary to photoisomerization in these molecules. Dube and coworkers have considered eight HTI derivatives with varying structural and electronic properties to decipher the parameters required to facilitate the ICT process in the excited state. The

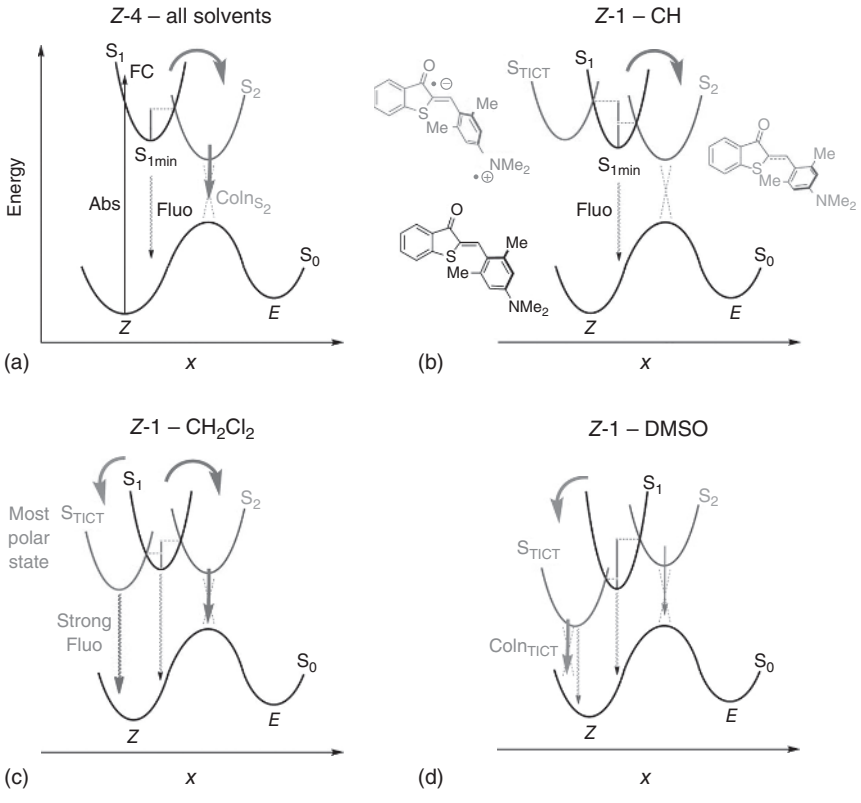

Figure 1.7 Schematic representation of excited-state deactivation mechanism of HTI derivatives: (a) *Z*-4 (in all solvents) and *Z*-1 (in cyclohexane, CH_2Cl_2 and DMSO). (Wiedbrauk *et al*. 2016 [45]. Reproduced with permission of American Chemical Society.)

HTI derivatives have different substitutions at the stilbene fragment and the twist angles around the rotatable single bond connecting the stilbene moiety with the photoisomerizable double bond are also different. HTI derivatives with acronyms *Z*-1 and *Z*-2 have strong donor units in conjugation with the photoisomerizable double bond. They also have large twisting of the stilbene fragment in the ground state. In all the HTI molecules used in this study, the thioindigo fragment with its strong electron-withdrawing carbonyl is used as the electron acceptor. HTI derivatives *Z*-3 and *Z*-4 possess strong donor groups but they are planar in the ground state. *Z*-5 and *Z*-6 do not possess strong electron-donating groups, although they are severely twisted around the rotatable single bond in their respective ground states. HTI derivatives *Z*-7 and *Z*-8 have substituents with moderate donating strength and they are twisted in the ground state. The authors argued that the varying donor strengths of the molecules studied can alter the push–pull character of the molecules, which is an important ingredient for formation of the ICT state. The steady-state electronic absorption spectra of *Z*-1 and *Z*-2 showed redshift in their absorption maxima with the increase in polarity of the media, although the effect is rather smaller than their

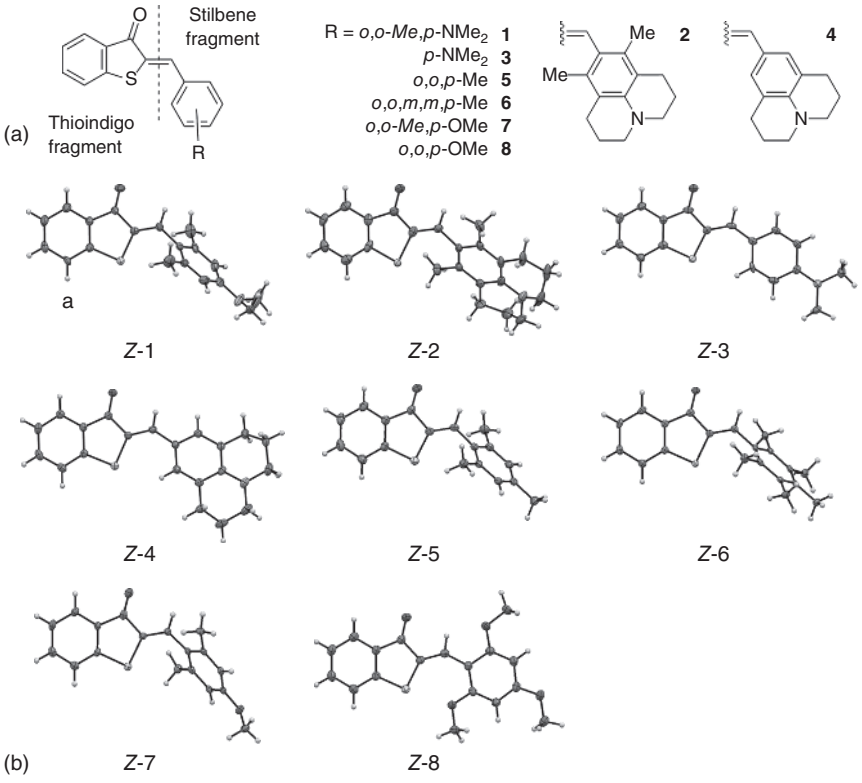

Figure 1.8 (a) Chemical structure of the HTI derivatives *Z*-1 to *Z*-8 studied by Dube and coworkers; (b) crystal structures of this *Z*-1 to *Z*-8. (Wiedbrauk *et al*. 2017 [49]. Reproduced with permission of American Chemical Society.)

corresponding emission spectra. The steady-state emission spectra of these derivatives showed strong bathochromic (red) shifts with increasing solvent polarity and occurrence of dual emission in solvents with large polarities. The planar derivatives *Z*-3 and *Z*-4 showed prominent solvent response, although much less compared to that of *Z*-1 and *Z*-2. The authors found that the effect of solvent polarity on the absorption and emission maxima of *Z*-5 and *Z*-6 are even smaller than that of *Z*-3 and *Z*-4. In spite of having twisted ground-state structures and donating groups with moderate strengths, the solvatochromic response of *Z*-7 and *Z*-8 are not very strong. Since the effect of solvent polarity on the emission energy is larger than the corresponding absorption energy of the molecules studied, the authors argued that the excited-state minima from which the fluorescence occurs are more polar than the FC region. As TICT is an alternative yet independent pathway of de-excitation along with the *Z*/*E* isomerization and the TICT process is highly dependent on the polarity of the solvents, it is expected that the quantum yield of *Z*/*E* photoisomerization will decrease significantly with increasing solvent polarity. In fact, the authors have used the quantum yield of *Z*/*E* photoisomerization ($\phi_{Z/E}$) as a tool for identification of the TICT process.

The HTI derivatives *Z*-1 and *Z*-2 show high $\phi_{Z/E}$ values in apolar solvents like cyclohexane, where no TICT is expected to occur. The values of $\phi_{Z/E}$ of these two compounds decrease with increasing solvent polarity, indicating formation of the TICT state. The $\phi_{Z/E}$ values for HTIs *Z*-3 and *Z*-4 also decrease with increases in solvent polarity, although the change is much lower than that of *Z*-1 and *Z*-2. The authors found that the $\phi_{Z/E}$ values for *Z*-5 to *Z*-8 were almost independent of the solvent polarity. The quantum yields of fluorescence of these derivatives are reported to be low irrespective of solvent polarity. The authors carried out time-resolved absorption spectroscopic measurements to explore TICT formation in the HTI derivatives. They noted that the TICT state in the HTI compounds were characterized by redshifted ESA and stimulated emissions that decay significantly slower than the initially populated excited-state minimum. In addition, the lifetime of the TICT state gets shortened with increasing solvent polarity. Time-resolved spectral data of *Z*-1 and *Z*-2 clearly indicated the formation of TICT in these compounds, while no evidence of TICT formation was observed in HTI derivatives *Z*-3 to *Z*-8. So, from their studies the authors conclude that although HTI derivatives *Z*-3 and *Z*-4 showed some indication of the TICT formation as indicated in decreasing values of $\phi_{Z/E}$ with solvent polarity, a complete study rules out formation of TICT in these molecules. No evidence of TICT formation was also observed in other HTIs (*Z*-5 to *Z*-8). Therefore, the authors conclude that considerable pretwisting of the stilbene fragment along with very strong donor group are required for the TICT to occur in the HTI derivatives reported in their study. From the nonoccurrence of TICT in HTI derivatives other than *Z*-1 and *Z*-2, although some of them possess pretwisted ground state and moderately strong donor groups, the authors infer that either of the aforesaid conditions are not enough for formation of TICT in these molecules.

The studies of ICT in 2-arylbenzotriazoles (Figure 1.9) by Turro and coworkers [50] also underscored the need for twisting of donor/acceptor groups for formation of the excited TICT states. The authors explored the ability of the aforesaid molecules as ultraviolet absorbers (UVAs) that dissipate the excited-state energy rapidly without any irreversible photochemistry. The quantum yields of decomposition of the UVAs are extremely low (in the order of 10^{-6} or even less), which renders them with unusual photostabilities. 2-(2-Hydroxy-5-methylphenyl)benzotriazole, also known as Tinuvin P, showed exceptional photostability due to efficient deactivation of excited singlet state through ESIPT process. Substitution of a methyl group at the 6′-position of 2-arylbenzotriazoles endowed the excited molecule with another deactivation mechanism. The authors undertook steady-state absorption and emission as well as time-resolved emission spectral studies to decipher the excited singlet state deactivation mechanism of 6′-methyl-2-arylbenzotriazoles that indicated the new process to be TICT. Their studies also revealed that due to steric requirement of the 6′-methyl group the TICT process was more facile in the molecules in which the phenyl and triazole rings were not in coplanar arrangements.

The authors installed two important features to the 2-arylbenzotriazole compounds to enhance the possibility of formation of excited TICT state. One of them is incorporation of methyl group in the 6′-position that provided an

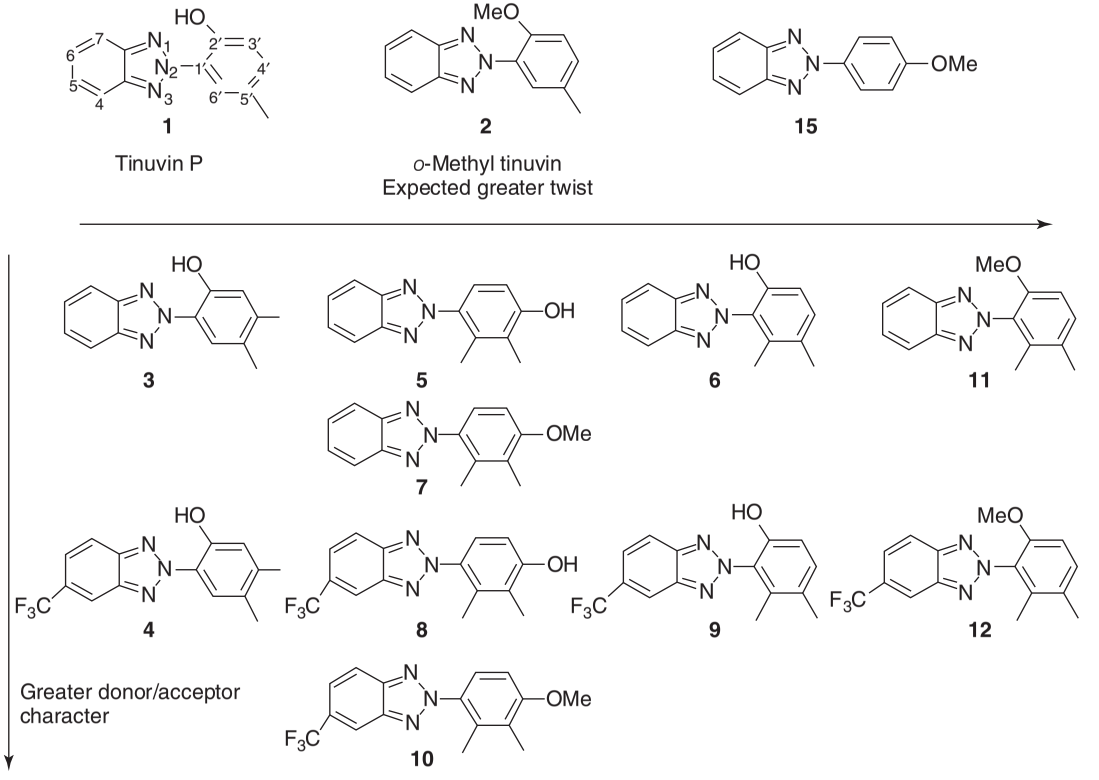

Figure 1.9 Chemical structures of the molecules studied by Turro and coworkers. The molecules were ordered on the basis of expected degree of twist along the triazole C—N bond as well as their donor/acceptor character. (Maliakal *et al.* 2002 [50]. Reproduced with permission of American Chemical Society.)

extra propensity of twisting in these molecules, while the other is addition of trifluoromethyl group to the triazole ring to increase their overall donor/acceptor character. They also explored the degree of twist on the formation of the TICT state by varying the substitution pattern. Their investigation revealed that the excitation led the molecule to the LE state (also FC state) which rapidly twisted to undergo the ICT process through which the TICT state was formed. The deactivation of the TICT state occurred through internal conversion either via a close approach or through a conical intersection with the ground state. In the framework of TICT, the rotation around the bond connecting the donor and the acceptor moieties that leads to the decoupling of the orbitals of these two groups occurs. This orbital decoupling could facilitate almost complete charge transfer in the molecule from the donor to the acceptor moiety, resulting in a highly polar twisted excited state. This polar excited state gets stabilized preferentially in solvents with high polarity, compared to its planar LE counterpart. As twisting makes the molecule energetically destabilized in the ground state, the formation of the excited TICT state brings the ground and excited states closer, which facilitates better internal conversion. The authors noted that although the donor/acceptor character was important, the degree of twist was a more important parameter for the TICT deactivation in these molecules. Several spectroscopic studies led the authors to conclude that the 2-(hydroxy or methoxy-6′-methylaryl)benzotriazoles could form the excited TICT state and the deactivation through the charge-transfer pathway accelerated the internal conversion from the TICT state to the ground state. They found that the compound with both twisting and strong donor/acceptor character (compound **12**) showed the most efficient fluorescence quenching. The compounds possessing both 6′-methyl and hydroxy groups on the phenyl ring showed diffusion-controlled quenching in DMSO solvent. The authors argued that the quenching process could be resulting from either partial or complete excited-state proton transfer to DMSO that enhances the deactivation of the singlet excited state through the TICT process.

As mentioned earlier, the debate regarding the structure of the excited state of ICT molecules is a matter of active debate in the scientific community. There are reports in the literature that the excited state can be planar as well. For example, Ghosh and coworkers [51] reported a novel concept to design planar (they call them "zero-twist" donor–acceptor molecules) ICT molecules for obtaining emission from both the solution and solid states. The authors took the help of quantum chemical calculations at the DFT (B3LYP functional/6-31G(d) basis set) level of theory. Their aim was to utilize the efficient segregation of highest occupied molecular orbital–lowest occupied molecular orbital (HOMO–LUMO) charge densities without the need for twisting of the donor and acceptor groups.

The authors [51] mentioned earlier studies that reported that planar emitters could suffer from an aggregation-caused quenching (ACQ), mostly due to face-to-face stacking as well as intramolecular interactions [52]. They also noted that the structural planarity, stacking modulator, and conformational rigidity were the major requirements for dual-state (solution and aggregate) emission from small molecules. Several organic donor–acceptor systems give rise to the TICT state, which may be weakly fluorescent or even nonfluorescent in

solvents, limiting their application in the solution phase. Therefore, to avoid the formation of the "dark" TICT state, the authors have envisioned molecules with a planar excited state that would be fluorescent in the solution as well as in their aggregated state. Using their quantum chemical studies, the authors proposed an ICT molecule possessing butterfly-shaped phenothiazine as electron donor group and oxazole as electron acceptor, which are connected through a covalent bond. They called the system as D-π^0-Ψ^0-A system as the system was zero-twist ($\Psi = 0$) and there was no additional π-spacer. The authors found that the allowed orbital overlap in the compounds studied was responsible for their solution-state fluorescence properties. Their molecular-level studies using single-crystal analysis pointed out the detrimental effects of intermolecular short-range forces on the solid-state emission properties of compound **1**. Therefore, they introduced an anisole group as bulky substitution to subtle stacked packing of compound **2**. The solid-state emission properties of the aforesaid compounds were studied by fabricating green-emitting devices of those compounds in unoptimized devices for OLED applications. As mentioned earlier, the authors undertook quantum chemical calculations to predict the zero-twist molecules with dual-state emitters. Their theoretical calculations showed that the oxazole moiety shared the plane of the phenothiazine unit and there was no distortion between those two units. In compound **2**, the only distortion was due to the presence of the anisole group. The authors envisioned that the π-stacking of compound **2** in solid state could be avoided with the help of non-planarity of the anisole group and the butterfly shape of the phenothiazine moiety. They found that both the compounds showed similar distribution of HOMO and LUMO energy levels and the presence of the anisole group in compound **2** did not affect the HOMO and LUMO levels of the molecule due to the high dihedral angle (96.8°) with the phenothiazine plane. In the aforesaid compounds, the maximum contribution to the HOMO and LUMO came from the phenothiazine and oxazole units, respectively. Therefore, charge transfer from the phenothiazine unit to oxazole unit could be observed upon photoexcitation. Natural transition orbital (NTO) analyses carried out by the authors indicated similar hole and particle distribution behavior. The excited-state geometries optimized at the DFT [B3LYP/6-31G(d)] level of theory predicted the planarization of the first excited states (S_1) of compounds **1** and **2** in which the butterfly bend of the phenothiazine unit became fully planar (Figure 1.10). These results led the authors to infer that the excitation energy dissipated to attain more planar structure in the excited state, thereby making the twisting around the single bond connecting the donor and acceptor units less favorable. Their emission quantum yield measurements also supported the formation of planar excited state. The quantum yields of emission of compounds **1** and **2** were 0.7 and 0.9 in DMSO, while those were 0.5 and 0.4 in dichloromethane (DCM), respectively. They related the increase in quantum yields with increasing solvent polarity to the rigidification of the conformations that resulted in loss of vibrational motions [53]. To understand the excited-state properties of compounds **1** and **2** more extensively, the authors carried out femtosecond TA measurements in acetonitrile medium. They used a 410-nm laser source of 35 fs pulse duration and measured the TA spectra of both the compounds at different pump probe delays.

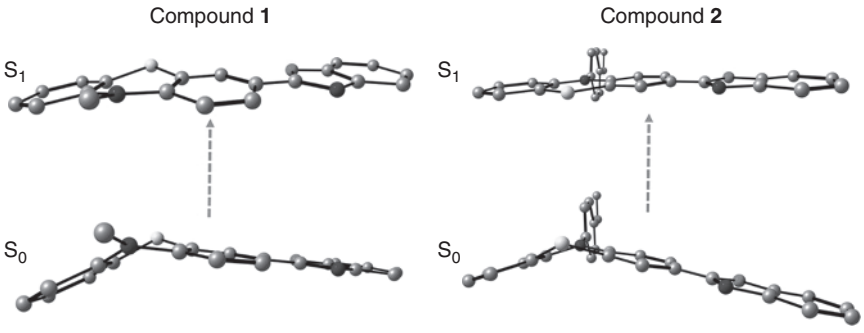

Figure 1.10 The ground- (S_0) and first-excited state (S_1) optimized structures of compounds **1** and **2**, studied by Ghosh and coworkers (Kumar *et al*. 2016 [51]. Reproduced with permission of American Chemical Society.)

The TA measurements revealed positive absorption bands in the 450–700 nm region with peaks at 550 and 525 nm for compounds **1** and **2**, respectively. They attributed these absorption bands to the ESA of those compounds. A gradual blueshift of the maximum of the absorptions bands was observed for both the compounds upon increasing delay of the pump-probe pulses up to 3 ps, while no such shift was observed thereafter. The aforesaid behavior (blueshift of TA bands) could be observed due to stabilization of the ICT excited states through solvation or geometrical relaxation of the molecules in the excited state [54, 55]. The authors also measured the TA kinetics at the ESA maxima of the compounds and fitted them with a biexponential function that consists of a rise and a decay component. They attributed the growth component with 667 fs lifetime to the solvent relaxation of the excited state, although they did not exclude the possibility of involvement of geometrical or vibrational (FC state) relaxation. The time constant (decay component) of 376 ps was assigned to the decay of the excited state back to the ground state of compound **1**. The authors argued that the relatively slower nature of the decay component could be due to the non-twisting of the excited state. Therefore, the results obtained from the TA studies supported the observation made from quantum chemical studies that the excited states of these compounds were planar in nature. The authors fabricated multilayer fluorescent OLED devices to evaluate their compounds for light-emitting applications. They used the compounds **1** and **2** as emissive layers in their unoptimized preliminary devices and compared their performances. Electroluminescence spectra and current–voltage–luminescence (*J–V–L*) characteristics of both the devices were examined. The color purity in the device using compound **2** was attributed to the relatively lesser intermolecular interaction, compared to that of compound **1**. Therefore, from the device application studies the authors inferred that the zero-twist D-π^0-Ψ^0-A emitter made of compound **2** could be used for designing organic emitters developed from the ACQ system. The molecular-level studies performed by the authors also underscores the role of steric bulkiness to avoid stacking in compound **2** that increased its emission quantum yield, compared to that of compound **1**.

1.3 Applications of ICT Molecules

The ICT-based molecules have been studied for potential applications in OLEDs, bioimaging applications through aggregation-induced emission (AIE), sensor for polarity and viscosity, and so on. As mentioned earlier, the ICT process is a fluorescence deactivation process which makes these molecules ready for potential use as UVAs. UVAs dissipate the excited-state energy quickly without the need for any irreversible photochemical reactions. Therefore, several studies that utilize ICT molecules to design UVAs have been reported in literature [56–58]. Interest in studies of OLEDs has been fueled as they provide several advantages over the conventional LEDs in terms of power consumption, big area fabrication compatibility, wide-viewing angle, fancy architecture, lightweight, higher brightness and sharper image, and so on [59]. ICT through which ultrafast deactivation of excited molecule could occur has been exploited in applications as laser dye absorbers that could be used in mode-locked lasers [60].

Teran and Reynolds [61] reported the designing strategies for using donor–acceptor conjugated systems in their neutral and oxidized states for use in high-contrast electrochromics. They mentioned that the conjugated molecules and polymers can be used for several technological applications as the structure and properties of these materials could be modulated with ease using myriad techniques of synthetic organic chemistry. One of the well-known methods is to link electron-rich and electron-deficient heterocycles covalently to prepare multi-ring molecules or copolymerized in such a way that an ICT interaction is induced. The aforesaid technique has been used by several research groups to design low-energy gap materials for light absorption in solar cells [62, 63], to develop materials with dual-band absorption [64], and so on. In electrochromics, the differences in the absorption/transmission properties of the neutral and charged species of a conjugated system is accessed through application of voltage and compound that shows sufficient contrast can be used in displays and smart windows. It is worth noting here that for several electronic applications, the absorption properties of the both the neutral and charged states should be situated within specific regions of the EM spectrum. Teran *et al*. have reported the neutral and oxidized state absorption and spin properties of a family of donor–acceptor–donor (D-A-D) molecules based on electron-rich dioxythiophenes (DOTs), electron-deficient 2,1,3-benzothiadiazole (BTD) and the heterocycles function as building blocks for electrochromic materials. They also studied the polymer with discrete D-A-D conjugated system obtained from the aforesaid units. They examined the steric and electronic structural requirements for designing high-contrast electrochromics and also proposed a method to translate the small conjugated molecules into polymeric materials that retain their well-defined properties for practical applications. The authors synthesized the three-, five- and seven-heterocycle conjugated molecules based on DOT and BTD units. They found that all the materials showed well-defined dual-band absorptions in the neutral state, arising from the charge-transfer interaction and the π–π^* high-energy excitation. The oxidized state generated through chemical and electrochemical doping took a structure in which the positive charge was

localized in the donor unit and the acceptor ring served as conjugation break. In penta-heterocycle (EPBPE), this led the polaron pair and its π-dimer to be the dominant charge carriers in the low- as well as high-oxidation states. In hepta-heterocycles (EPPBPPE), the longer donor segment generated polaron pairs with significantly redshifted absorption with peak outside the visible region. The authors found that the extended structure allowed formation of bipolarons at higher doping levels. The absorption maxima of both the charge carriers were in the near-IR region. They designed polymers of the aforesaid D-A materials by linking the units through aliphatic chains. Although poly-EPBPE showed well-defined and narrow transitions in its absorption spectra, in higher oxidation states the effect of π–π interactions became significantly higher. This led the authors to propose that one needs to design the linker carefully (like sterically bulky aliphatic groups) to develop polymeric materials that are devoid of undesired interactions from discrete chromophores.

Of late, several ICT-based molecules are being used as fluorescent and colorimetric sensors as well as NLO switches. Novel ICT-based molecules are being designed to detect ions and molecules in solution as well as in living cells. Applications of ICT probes in AIE, dye-sensitized solar cells, and OLEDs are also being reported. Some of these applications are discussed in Chapters 5 and 6. We have already mentioned that the dipole moment of a charge-transfer molecule could be higher in the exited state than in the ground state, leading to a bathochromic shift in its electronic absorption spectrum. A simple two-state model, proposed by Ouder [65, 66] suggests that the ICT molecules may possess high quadratic first hyperpolarizability, a term used to quantize the first-order NLO response. The NLO response property of a material is ultimately shaped by the NLO response of the individual chromophores, sometimes referred to as the building blocks. A high first hyperpolarizability from a single chromophore is generally taken as a signature of a low-lying ICT state in the building block. Tuning of the ICT process of a molecule is therefore an essential ingredient in the designing of materials with high NLO response. It has been reported by many research groups that organic molecules with ICT can be possible chromophores for NLO materials. According to the two-state model proposed by Ouder [65, 66], the static or field-independent first hyperpolarizability (β) of the system can be calculated using Equation 1.2.

$$\beta_0 = \frac{3}{2}\left[\frac{\Delta\mu f_0}{(\Delta E)^3}\right] \tag{1.2}$$

where ΔE is the difference in energy between the ground and excited states of a molecule, while the f_0 stands for the oscillator strength of the transition. The term $\Delta\mu$ represents the difference in dipole moments between the ground and excited states of the molecule.

From Ouder's model one can therefore anticipate that the molecules having high HOMO–LUMO energy gap and large values of $\Delta\mu$ can result into high second-order NLO response. Although the NLO response of a material is measured using experimental techniques like electric-field–induced second harmonic generation (EFISH), Z-scan, hyper-Rayleigh scattering (HRS), and so on, the polarizability and hyperpolarizabilities (β_0) are the properties of

a free molecule. The values of the polarizability (α) and hyperpolarizabilities (β, γ, ..) are independent of the material and can be calculated using quantum chemical techniques. Due to availability of vast literature, we have separated the application of ICT molecules for NLO response from other applications and discussed it in little more detail in Chapter 5. Two-photon absorption (TPA), another nonlinear phenomenon has drawn the interest of the scientific community for possible technological applications of TPA-based materials. Several ICT-based molecules have been examined recently for preparation of materials with high TPA activities. The basic theory behind the calculations of polarizability and hyperpolarizabilities of a molecule are also discussed in the same chapter (Chapter 5). *para*-Nitroaniline (PNA) is the one of the very first organic molecules that showed very high NLO response. Later on, several molecules with ICT were explored for designing possible NLO materials [67–78]. Till date, most of the NLO studies concern the second-order NLO response, while few reports of third-order NLO response have been reported in literature. Some representative examples of studies of second- and third-order NLO response and TPA properties of ICT-based molecules are discussed in Chapter 5. It is worth mentioning that the choice of theoretical method is important to accurately calculate the polarizability and hyperpolarizabilities of a molecule [79–85]. Electron correlation is reported to be an important parameter for calculations of linear and NLO response properties of a molecule [86, 87]. The vibrational contribution and effect of the medium are other two interesting topics for studies of NLO response [88]. As expected, several studies have been reported in literature concerning these issues. Coupled cluster singles and doubles (CCSD) and coupled cluster singles and doubles with a perturbative estimate of triples [CCSD(T)] level of theories have been used to calculate the polarizabilities and hyperpolarizabilities of several relatively small molecules, while using these theories for larger molecules are costly [85]. Therefore, several alternate methodologies have been adopted by the scientific community to reproduce the experimental values of α, β, and γ with some approximations. For ICT-based molecules, use of MP2 theory seems to be one of the popular choices. Several DFT functionals and basis sets have been designed to calculate the values of α, β, and γ of conjugated molecules [85].

Champagne and coworker [81] studied the effect of electron correlation on the first hyperpolarizability of a number of push–pull π-conjugated molecules (Figure 1.11). They found the 6-31+G(d,p) basis set gave a balance between the computational resources and accuracy for the polyene linkers. The authors reported that due to cancellation between higher order contributions the MP2 method was most accurate in predicting the values of β of push–pull polyene molecules as the values closely reproduced those obtained through CCSD(T) calculations. In case of exchange-correlation DFT functionals, the authors found the LC-BLYP was reliable while predicting the changes of β while enlarging the π-conjugation network or upon changing the polyene linker to a polyene segment, although its reliability is reported to be close to that of HF method and MP2 method was far superior.

Luthi and coworkers [86] reported their theoretical investigation of polarizability and second hyperpolarizability of polyacetylene oligomer chains with

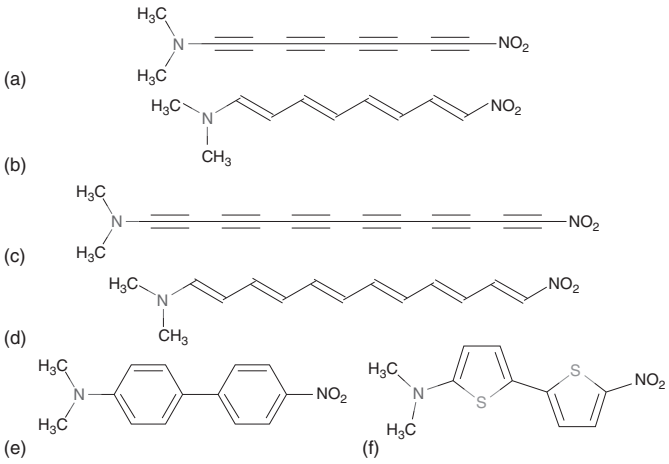

Figure 1.11 Chemical structures of π-conjugated donor–acceptor molecules studies by Champagne and coworkers. (de Wergifosse and Champagne 2011 [81]. Reproduced with permission of American Institute of Physics.)

increasing size up to $C_{24}H_{26}$. These polyacetylenes are prototypical systems for studying the π-conjugation in a linear framework and the interactions between the adjacent double bonds can be tuned through incorporation of electron donor and acceptor groups at two ends. The authors used long-range corrected CAM-B3LYP functional for calculation of α and γ of a series of polyacetylenes and compared the theoretically estimated values with that obtained experimentally. They found this functional could remove the large part of overestimation generally observed using standard DFT methods and even in some cases the values are close to coupled cluster calculations. They found that CAM-B3LYP reproduced the structure of the molecules found experimentally and was found better than the standard B3LYP functional and MP2 method. The authors reported that the experimental values of second hyperpolarizability of ethylene, butadiene, and hexatriene could be reproduced, although they found CAM-B3LYP and CCSD generally overestimated the values by 25% and 10%, respectively.

Several molecules exhibit structural changes in response to external stimuli like changing polarity and acidity/basicity (pH) of the medium, irradiating the sample with light of specific frequency, the temperature of the system, the redox potential, and so on [87–89]. If these alterations lead to spectral changes (generally in the visible region but not always), then the molecules are referred to as photochromes, thermochromes, and acidochromes, when the changes are induced by irradiation, changing temperature, and acidity of the medium, respectively. Some properties of these compounds can be tuned reversibly to achieve "on" and "off" states that could be useful in devices such as sensors, actuators, memory, and so on. Similar to change in linear absorption and emission maxima of the probe, the external stimuli can also change the NLO properties of a molecule, such as second-harmonic generation (SHG), third-harmonic generation, and TPA [90, 91]. Molecules in which the structural change triggers

changes in NLO response properties are called NLO switches. A vast majority of the NLO switches exhibit changes in their first hyperpolarizability (β), which is the molecular property at the origin of SHG. Although the change in β with structural changes were observed in several molecules, including azobenzenes, nitrobenzylpyridines, diarylethenes, *N*-salicyclidene-aniline, and spiropyrans, several organometallic complexes with Fe, Ru, Zn, and Pt transition metal atoms, and, indolinooxazolidine and spiropyran derivatives were shown to behave as highly efficient NLO switches that showed large differences in their NLO responses due to structural changes induced through external stimuli [89].

OLEDs usually consist of ultrathin layers of soft and amorphous organic semiconductors [92]. OLEDs are believed to be potential candidates for next-generation displays and solid-state lighting owing to their low driving voltage, high brightness, and high efficiency. These devices can also realize the extreme wide viewing and high color quality. The compatibility with production processes has made these devices attractive for the scientific community. Solution processing is believed to be the most favorable method for fabrication of OLED devices for low-cost and large-area applications [93]. Once the fluorescence is switched on, the holes and electrons are fed into the organic semiconductor in which they bind together to form the excitons [92]. These excitons are generally localized on single molecules and carry a distinct spin character. It can be either a singlet state, which is light emitting, or a triplet state, which is non-radiative. It has been reported that due to unfavorable spin statistics, for every singlet state that is created, three triplet states will also be created. That is, the population of singlet and triplet states will be 25% and 75%, respectively. As these triplet states are non-emissive, this will lead to loss of about two-thirds of the total energy that limits use of organic semiconductors for OLED applications. The problem of unfavorable spin statistics was taken care of using phosphorescence-based molecules as emitters. In these devices, heavy metal ions such as iridium and platinum that leads to strong spin–orbit coupling (SOC) within the molecule are introduced. The SOC process leads to fast and efficient transition from singlet to triplet state (called intersystem crossing) and also enhances the transition from the triplet to the ground state (called phosphorescence). This method forces the system to luminescence from the triplet state, irrespective of the initial spin state of the excitons, offering a theoretical internal quantum efficiency of cent percent. However, the applications of phosphorescence-based materials are limited by their high cost due to use of precious metals. Adachi and coworkers have introduced the concept of thermally activated delayed fluorescence (TADF) to overcome the unfavorable spin statistics in organic materials [94]. The TADF method relies on reverse intersystem crossing from the triplet state to the radiative singlet state. They have shown that when the singlet and triplet states are close in energy, using the thermal energy at room temperature the triplets can transition to the singlet state, thereby making the internal quantum efficiency of the system to 100%. One of the key rules to design the system with very small gap between the singlet and triplet states (ΔE_{ST}) is to minimize the spatial overlap between the HOMO and LUMO of the molecule. ICT molecules, in which electron donor and acceptor groups are connected through a π-electron bridge, are used to prepare TADF molecules for OLED applications [95]. This

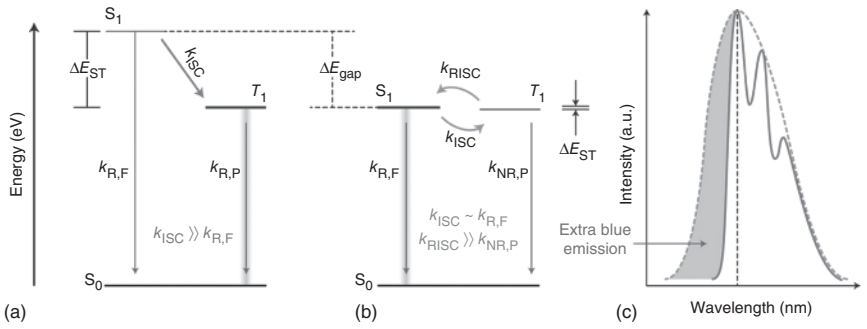

Figure 1.12 Simplified Jablonski diagrams for (a) phosphorescence- and (b) TADF-based emitters. The difference between the spectral distributions of phosphorescence (dashed curve) and TADF emissions (solid curve) are shown in (c). Important rate processes are indicated using arrows. In the figure R, NR, F, P, ISC, RISC, and ΔE_{ST} stand for radiative, non-radiative, fluorescence, phosphorescence, intersystem crossing, reverse ISC and singlet–triplet splitting energy, respectively. (Reineke 2014 [92]. Reproduced with permission of Macmillian Publishers Limited.)

is due to the fact that in ICT molecules the delocalization of π-electrons leads to separation of the HOMO and LUMO, thereby giving rise to small values of ΔE_{ST}. Adachi *et al*. have shown that in intermolecular charge-transfer complexes, the TADF process can be observed through separation of the wavefunction over a heterointerface between the molecules forming the complex. The difference between the phosphorescence-based emitters and TADF-based emitters has been shown in Figure 1.12.

From the preceding discussion it is apparent that ICT-based molecules have been used to design materials for applications in molecular switch, in nonlinear optics, in OLEDs, and so on. Some of these applications are discussed in detail in Chapter 6. Chapter 7 summarizes the studies presented in this book. Some of the unresolved issues concerning the ICT processes are also discussed.

References

1 Sedghi, G., Sawada, K., Esdaile, L.J., Hoffmann, M., Anderson, H.L., Bethell, D., Haiss, W., Higgins, S.J., and Nichols, R.J. (2008) *J. Am. Chem. Soc.*, **130**, 8582.

2 Closs, G.L. and Miller, J.R. (1988) *Science*, **240**, 440.

3 Bredas, J.L., Calbert, J.P., da Silva Filho, D.A., and Cornil, J. (2002) *Proc. Natl. Acad. Sci. U.S.A.*, **99**, 5804.

4 Barbara, P.F., Walker, G.C., and Smith, T.P. (1992) *Science*, **256**, 975.

5 Kobori, Y., Yamauchi, S., Akiyama, K., Tero-Kubota, S., Imahori, H., Fukuzumi, S., and Norris, J.R. (2005) *Proc. Natl. Acad. Sci. U.S.A.*, **102**, 10017.

6 Zhao, G.-J., Liu, J.-Y., Zhou, L.-C., and Han, K.-L. (2007) *J. Phys. Chem. B*, **111**, 8940.

7 Bulheller, B.M., Miles, A.J., Wallace, B.A., and Hirst, J.D. (2008) *J. Phys. Chem. B*, **112**, 1866.

8 Li, G., Josowicz, M., Janata, J., and Semancik, S. (2004) *Appl. Phys. Lett.*, **85**, 1187.
9 Arzhantsev, S., Zachariasse, K.A., and Maroncelli, M. (2006) *J. Phys. Chem. A*, **110**, 3454.
10 Cao, X., Tolbert, R.W., McHale, J.L., and Edwards, W.D. (1998) *J. Phys. Chem. A*, **102**, 2739.
11 Thar, J., Zahn, S., and Kirchner, B. (2008) *J. Phys. Chem. B*, **112**, 1456.
12 Akemann, W., Laage, D., Plaza, P., Martin, M.M., and Blanchard-Desce, M. (2008) *J. Phys. Chem. B*, **112**, 358.
13 Zyss, J., Ledoux, I., Volkov, S., Chernyak, V., Mukamel, S., Bartholomew, G.P., and Bazan, G.C. (2000) *J. Am. Chem. Soc.*, **122**, 11956.
14 Zachariasse, K.A. (2000) *Chem. Phys. Lett.*, **320**, 8.
15 Druzhinin, S.I. *et al.* (2010) *J. Am. Chem. Soc.*, **132**, 7730.
16 Grabowski, Z.R., Rotkiewicz, K., and Rettig, W. (2003) *Chem. Rev.*, **103**, 3899.
17 Tassel, A.J.V., Prantil, M.A., and Fleming, G.A. (2006) *J. Phys. Chem. B*, **110**, 18989.
18 Zhang, W., Lan, Z., Sun, Z., and Gaffney, K.J. (2012) *J. Phys. Chem. B*, **116**, 11527.
19 Schmuttenmaer, C.A. (2004) *Chem. Rev.*, **104**, 1759.
20 Kumpulainen, T., Lang, B., Rosspeintner, A., and Vauthey, E. (2017) *Chem. Rev.* doi: 10.1021/acs.chemrev.6b00491
21 Marcus, R.A. (1993) *Rev. Mod. Phys.*, **65**, 599.
22 Pelzer, K.M. and Darling, S.B. (2016) *Mol. Syst. Des. Eng.*, **1**, 10.
23 Paddon-Row, M.N. (2001) in *Electron Transfer in Chemistry* (ed. V. Balzani), Wiley-VCH Verlag GmbH & Co. KGaA, Weinheim.
24 Sumi, H. and Marcus, R.A. (1986) *J. Chem. Phys.*, **84**, 4894.
25 Manna, A.K. and Dunietz, B.D. (2014) *J. Chem. Phys.*, **141**, 121102.
26 Rettig, W., Bliss, B., and Dirnberger, K. (1999) *Chem. Phys. Lett.*, **305**, 8.
27 Rettig, W. (1986) *Angew. Chem. Int. Ed. Engl.*, **25**, 971.
28 Zilberg, S. and Haas, Y. (2002) *J. Phys. Chem. A*, **106**, 1.
29 Yoshihara, T., Druzhinin, S.I., and Zachariasse, K.A. (2004) *J. Am. Chem. Soc.*, **126**, 8535.
30 Gomez, I., Reguero, M., Boggio-Pasqua, M., and Robb, M.A. (2005) *J. Am. Chem. Soc.*, **127**, 7119.
31 Cogan, S., Zilberg, S., and Haas, Y. (2006) *J. Am. Chem. Soc.*, **128**, 3335.
32 Chu, G. and Yangbo, F. (1987) *J. Chem. Soc., Faraday Trans.*, **83**, 2533.
33 Sobolewski, A.J. and Domcke, W. (1996) *Chem. Phys. Lett.*, **259**, 119.
34 Barbara, P.F. and Jarzeba, W. (1988) *Acc. Chem. Res.*, **21**, 195.
35 Tavernier, H.L., Barzykin, A.V., Tachiya, M., and Fayer, M.D. (1998) *J. Phys. Chem. B*, **102**, 6078.
36 Kosower, E.M. and Huppert, D. (1983) *Chem. Phys. Lett.*, **96**, 433.
37 Li, X. and Maroncelli, M. (2011) *J. Phys. Chem. A*, **115**, 3746.
38 Samanta, A., Paul, B.K., and Guchhait, N. (2012) *J. Lumin.*, **132**, 517.
39 Brutschy, B. (2000) *Chem. Rev.*, **100**, 3891.
40 Zhao, G.-J., Chem, R.-K., Sun, M.-T., Liu, J.-Y., Li, G.-Y., Gao, Y.-L., Han, K.-L., Yang, X.-C., and Sun, L. (2008) *Chem. Eur. J.*, **14**, 6935.
41 Wasielewski, M.R. (1992) *Chem. Rev.*, **92**, 435.

42 Zhang, J., Xu, Q., Feng, Z., Li, M., and Li, C. (2008) *Angew. Chem.*, **120**, 1790.
43 Hara, K., Dan-oh, Y., Kasada, C., Yasuyo, O., Shinpo, A., Suga, S., Sayama, K., and Arakawa, H. (2004) *Langmuir*, **20**, 4205.
44 Nazarov, A.E., Malykhin, R., and Ivanov, A.I. (2017) *J. Phys. Chem. B*, **121**, 589.
45 Wiedbrauk, S., Maerz, B., Samoylova, E., Reiner, A., Trommer, F., Mayer, P., Zinth, W., and Dube, H. (2016) *J. Am. Chem. Soc.*, **138**, 12219.
46 Muraoka, T., Kinbara, K., and Aida, T. (2006) *Nature*, **440**, 512.
47 Gostl, R., Senf, A., and Hecht, S. (2014) *Chem. Soc. Rev.*, **43**, 1982.
48 Samanta, S., Qin, C., Lough, A.J., and Wolley, G.A. (2012) *Angew. Chem. Int. Ed.*, **51**, 6452.
49 Wiedbrauk, S., Maerz, B., Samoylova, E., Mayer, P., Zinth, W., and Dube, H. (2017) *J. Phys. Chem. Lett.*, **8**, 1585.
50 Maliakal, A., Lem, G., Turro, N.J., Ravichandran, R., Suhadolnik, J.C., DeBellis, A.D., Wood, M.G., and Lau, J. (2002) *J. Phys. Chem. A*, **106**, 7680.
51 Kumar, S., Singh, P., Kumar, P., Srivastava, R., Pal, S.K., and Ghosh, S. (2016) *J. Phys. Chem. C*, **120**, 12723.
52 Saigusa, H. and Lim, E.C. (1995) *J. Phys. Chem.*, **99**, 15738.
53 Chen, G., Li, W., Zhou, T. *et al* (2015) *Adv. Mater.*, **27**, 4496.
54 Fakis, M., Hrobarik, P., Yuschenko, O. *et al* (2014) *J. Phys. Chem. C*, **118**, 28509.
55 Bredas, J.L., Calbert, J.P., da Silva Filho, D.A., and Cornil, J. (2002) *Proc. Natl. Acad. Sci. U.S.A.*, **99**, 5809.
56 Paterson, M.J., Robb, M.A., Blancafort, L., and DeBellis, A.D. (2004) *J. Am. Chem. Soc.*, **126**, 2912.
57 Elbe, F., Keck, J., Fluegge, A. *et al* (2000) *J. Phys. Chem. A*, **104**, 8296.
58 Keck, J., Roesller, M., Schroeder, C. *et al* (1998) *J. Phys. Chem. B*, **102**, 6975.
59 Liang, J., Li, L., Niu, X., Yu, Z., and Pei, Q. (2013) *Nat. Photonics*, **7**, 817.
60 Vogel, M. and Rettig, W. (1985) *Ber. Bunsen Ges. Phys. Chem.*, **89**, 962.
61 Teran, N. and Reynolds, J.R. (2017) *Chem. Mater.*, **29**, 1290.
62 Zhou, H., Yang, L., and You, W. (2012) *Macromolecules*, **45**, 607.
63 Dow, L., Liu, Y., Hong, Z., Li, G., and Yang, Y. (2015) *Chem. Rev.*, **115**, 12633.
64 Baeujuge, P.M., Amb, C.M., and Reynolds, J.R. (2010) *Acc. Chem. Res.*, **43**, 1396.
65 Ouder, J.L. (1977) *J. Chem. Phys.*, **67**, 446.
66 Ouder, J.L. (1977) *J. Chem. Phys.*, **67**, 2664.
67 Albert, I.D.L., Marks, T.J., and Ratner, M.A. (1998) *J. Am. Chem. Soc.*, **120**, 11174.
68 Yang, G. and Su, Z. (2009) *Int. J. Quantum Chem.*, **109**, 1553.
69 Nandi, P.K., Panja, N., Ghanty, T.K., and Kar, T. (2009) *J. Phys. Chem. A*, **113**, 2623.
70 Ishow, E., Bellaiche, C., Bouteiller, L., Nakatani, K., and Delaire, J.A. (2003) *J. Am. Chem. Soc.*, **125**, 15744.
71 Wang, C.-K. and Yang, W.-H. (2003) *J. Chem. Phys.*, **119**, 4409.
72 Geskin, V.M., Lambert, C., and Bredas, J.L. (2003) *J. Am. Chem. Soc.*, **125**, 15651.

73 Albert, I.D.L., Marks, T.J., and Ratner, M.A. (1997) *J. Am. Chem. Soc.*, **119**, 6575.
74 Zyss, J. (1979) *J. Chem. Phys.*, **71**, 909.
75 Lacroix, P.G., Padilla-Martinez, I.I., Sandoval, H.L., and Nakatai, K.N. (2004) *New J. Chem.*, **28**, 542.
76 Marder, S.R. and Perry, J.W. (1993) *Adv. Mater.*, **5**, 804.
77 Kang, H., Facchetti, A., Jiang, H., Cariati, E., Rietto, S., Ugo, R., Zuccaccia, C., Macchioni, A., Stern, C.L., Liu, Z., Ho, S.-T., Brown, E.C., Ratner, M.A., and Marks, T.J. (2007) *J. Am. Chem. Soc.*, **127**, 3267.
78 Dehu, C., Meyers, F., Hendrickx, E., Clays, K., Persoons, A., Marder, S.R., and Bredas, J.L. (1995) *J. Am. Chem. Soc.*, **117**, 10127.
79 Champgne, B. (2009) in *Polarizabilities and Hyperpolarizabilities in Chemical Modeling*, vol. **6** (ed. M. Springborg), Royal Society of Chemistry, London.
80 Maroulis, G., Bancewicz, T., and Champagne, B. (eds) (2011) *Atomic and Molecular Nonlinear Optics: Theory, Experiment and Computation: A Homage to the Pioneering Work of Stanisław Kielich (1925–1993)*, IOS Press, Amsterdam.
81 de Wergifosse, M. and Champagne, B. (2011) *J. Chem. Phys.*, **134**, 074113.
82 Zhang, L., Qi, D., Zhao, L., Chen, C., Bian, Y., and Li, W. (2012) *J. Phys. Chem. A*, **116**, 10249.
83 Bai, Y., Zhou, Z.J., Wang, J.J., Li, Y., Wu, D., Chen, W., Li, Z.R., and Sun, C.C. (2013) *J. Phys. Chem. A*, **117**, 2835.
84 Karamanis, P. and Maroulis, G. (2011) *J. Phys. Org. Chem.*, **24**, 588.
85 Alparone, A. (2013) *Chem. Phys. Lett.*, **563**, 88.
86 Limacher, P.A., Mikkelsen, K.V., and Luthi, H.P. (2009) *J. Chem. Phys.*, **130**, 194114.
87 Berkovic, G., Krongauz, V., and Weiss, V. (2000) *Chem. Rev.*, **100**, 1741.
88 Zhang, J., Zou, Q., and Tian, H. (2013) *Adv. Mater.*, **25**, 378.
89 Beaujean, P., Bondu, F., Plaquet, A., Garcia-Amoros, J., Cusido, J., Raymo, F.M., Castet, F., Rodriguez, V., and Champagne, B. (2016) *J. Am. Chem. Soc.*, **138**, 5052.
90 Castet, F., Rodriguez, V., Pozzo, J.-L., Ducasse, L., Plaquet, A., and Champagne, B. (2013) *Acc. Chem. Res.*, **46**, 2656.
91 Delaire, J.A. and Nakatani, K. (2000) *Chem. Rev.*, **100**, 1817.
92 Reineke, S. (2014) *Nat. Photonics*, **8**, 269.
93 Burroughes, J.H., Bradley, D.D.C., Brown, A.R., Mackay, R.N., Marks, K., Friend, R.H., Burns, P.L., and Holmes, A.B. (1990) *Nature*, **347**, 539.
94 Nakanotani, H., Masui, K., Nishide, J., Shibata, T., and Adachi, C. (2013) *Sci. Rep.*, **3**, 2127.
95 Endo, A. *et al* (2009) *Adv. Mater.*, **21**, 4802.